

Accurate effective pair potentials for polymer solutions

P.G. Bolhuis, A.A. Louis, and J.P. Hansen

Department of Chemistry, Lensfield Rd, Cambridge CB2 1EW, UK

E.J. Meijer

Department of Chemical Engineering, University of Amsterdam, Nieuwe Achtergracht 166, NL-1018 WV Amsterdam, Netherlands.

(March 21, 2022)

Dilute or semi-dilute solutions of non-intersecting self-avoiding walk (SAW) polymer chains are mapped onto a fluid of “soft” particles interacting via an effective pair potential between their centers of mass. This mapping is achieved by inverting the pair distribution function of the centers of mass of the original polymer chains, using integral equation techniques from the theory of simple fluids. The resulting effective pair potential is finite at all distances, has a range of the order of the radius of gyration, and turns out to be only moderately concentration-dependent. The dependence of the effective potential on polymer length is analyzed in an effort to extract the scaling limit. The effective potential is used to derive the osmotic equation of state, which is compared to simulation data for the full SAW segment model, and to the predictions of renormalization group calculations. A similar inversion procedure is used to derive an effective wall-polymer potential from the center of mass density profiles near the wall, obtained from simulations of the full polymer segment model. The resulting wall-polymer potential turns out to depend strongly on bulk polymer concentration when polymer-polymer correlations are taken into account, leading to a considerable enhancement of the effective repulsion with increasing concentration. The effective polymer-polymer and wall-polymer potentials are combined to calculate the depletion interaction induced by SAW polymers between two walls. The calculated depletion interaction agrees well with the “exact” results from much more computer-intensive direct simulation of the full polymer-segment model, and clearly illustrates the inadequacy – in the semi-dilute regime – of the standard Asakura-Oosawa approximation based on the assumption of non-interacting polymer coils.

I. INTRODUCTION

Polymer solutions have attracted the attention of theorists and experimentalists alike for many decades, and a theoretical understanding of their structure and phase behavior, based on mean-field and on scaling or renormalization group arguments, is by now well established [1–6]. Recently, there has been a growing interest in the structure, phase behavior and rheology of binary systems involving colloidal particles and non-adsorbing polymer [7–22]. In such mixtures the mean size of the polymer coils, i.e. their radius of gyration R_g , is comparable to, or smaller than the diameter σ of the colloidal particles. Since the latter may, for most purposes, be modeled as “hard” convex bodies dominated by excluded volume effects on the mesoscopic scale σ , it is clear that a statistical description of the polymer coils requires a high degree of coarse-graining to provide a tractable theory of these mixtures. Such coarse-graining is, more generally, desirable for theoretical investigations of large scale phenomena involving large numbers of interacting polymer chains in the dilute or semi-dilute regimes. In particular, simulations of solutions involving many interacting polymer chains become rapidly intractable if a detailed description at the level of monomers or even of Kuhn

segments is retained. It is therefore tempting to consider polymer coils as “soft” particles, and to replace the detailed interactions between segments by an effective interaction acting between the centers of mass (CM) of different polymer coils as shown schematically in Fig. 1.

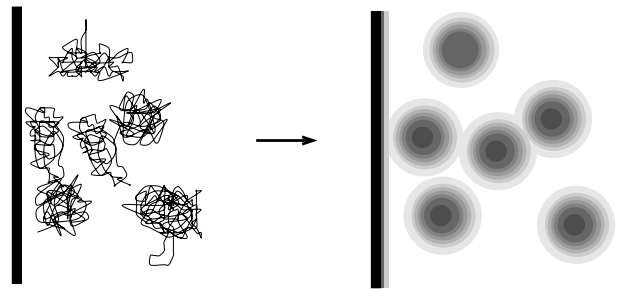


FIG. 1. Modelling polymer coils by effective “soft particles”. The N polymers, each made up of L segments, are replaced by N particles interacting with an effective pair potential. The centers of the particles correspond to the polymer CM. The interaction of the polymers with a hard wall is modelled by a single soft particle–wall interaction.

Similarly, an effective interaction must be worked out between the “soft” polymer coils and the “hard” colloidal particles. Such a drastic reduction in the number of degrees of freedom, achieved by formally averaging over the

coordinates of individual polymer segments, leads to a considerable simplification of the initial problem involving N_c colloidal particles and $N_p L$ polymer segments, where N_p is the number of polymer coils and L the number of monomers or segments per polymer (i.e. the length of a polymer). The idea of representing a polymer coil by a single particle of radius of the order of R_g goes back to the work of Flory and Krigbaum [23], who considered the infinite dilution limit of two isolated interacting polymers. A brief outline of subsequent theoretical and numerical work on the two-coil problem is given in Section III. In this paper we generalize the idea to finite concentrations, i.e. to dilute and semi-dilute polymer solutions. The effective interaction between the CM of polymer coils is determined by a combination of Monte Carlo (MC) simulations of a detailed segment model of interacting polymers, and of an inversion technique which allows the effective pair interaction to be extracted from the MC results for the center of mass pair distribution function. A similar inversion technique is applied to the density profiles of the CM of the polymers near a hard wall to determine the effective interaction between a wall, impenetrable to the polymer segments, and the CM of interacting polymers. The effective polymer-polymer and wall-polymer interactions provide a first step towards a complete description of colloid-polymer mixtures, with the hard wall considered in this paper representing a single colloidal particle of infinite radius. The ultimate goal is to go well beyond the familiar Asakura-Oosawa (AO) model which considers polymers to be non-interacting point particles, excluded from a sphere of radius $\sigma/2 + R_g$ around each colloidal particle [24]. This model leads to the well-known AO depletion interaction between hard sphere colloids [24–26]. As an application of the general method outlined in this paper, the limitations of the AO picture will be illustrated in a calculation of the depletion interaction between two parallel hard walls. The effective interaction between polymer coils will be shown to lead to considerable deviations from the AO results, even in the dilute regime.

A preliminary account of parts of the present work has been published elsewhere [27]. A related soft particle picture has recently been applied to polymer melts and polymer blends [28]. However, the phenomenological coarse-graining procedure proposed by these authors, and its practical implementation, differ considerably from the present “first principles” approach, which is better adapted to dilute and semi-dilute polymer solutions. Both methods are good examples of current efforts to bridge widely different length and time scales in complex fluids.

II. SIMULATION MODELS AND METHODS

Many physical properties of polymers in solution already emerge from simple models which ignore chemical detail and describe the polymers as self avoiding walks (SAW) with hard segments interacting through a simple potential. For example, solutions of linear polymers in a good solvent are well modeled by N athermal SAW’s, each made up of L non-intersecting segments, on a cubic lattice of M sites, with periodic boundary conditions. This model captures the leading scaling behavior and has been used for many decades to describe polymer solutions [1–6]. Slightly more sophisticated models exist, such as the fluctuating bond model [29] or off-lattice hard sphere chains [30], but the SAW lattice model is simple, efficient and allows for comparisons with previous studies.

Within the lattice model, the monomer packing fraction is equal to the fraction of lattice sites occupied by polymer segments, $c = N \times L/M$, while the concentration of polymer chains is $\rho_b = c/L = N/M$. For a single SAW chain, the radius of gyration scales as $R_g \sim L^\nu$, where $\nu \simeq 0.6$ is the Flory exponent [1]. The overlap concentration ρ^* , signalling the onset of the semi-dilute regime, is such that $4\pi\rho^*R_g^3/3 \simeq 1$, and hence $\rho^* \sim L^{-3\nu}$ [31].

To sample the configuration space of the polymer system we employ the Monte Carlo pivot algorithm [30,32] which attempts to rotate part of the polymer around a random segment (the pivot). If the new trial configuration shows no overlap, the move is accepted, otherwise the old configuration is restored. This simple scheme turns out to be very effective for single polymers and dilute polymer solutions where we found that it efficiently samples configurational space up to densities $\rho_b/\rho^* \approx 1$ for $L = 500$ polymers. Because the polymers are restricted to a cubic lattice, the pivot move can only take place in 5 possible directions. For efficiency we store the complete lattice in memory, so that overlap between different polymers can be easily checked for. In this way one has only to check of order L sites per polymer move, which is much more efficient than the NL^2 sites needed when each pair of segments has to be tested for overlap.

In addition to the pivot moves, we also attempt to translate the polymer. This Monte Carlo move enhances the relaxation to equilibrium of the polymer solution, although the acceptance ratio for this move decreases rapidly if the density exceeds $\rho_b/\rho^* \approx 1$ (for $L = 500$ polymers). For densities deep in the semi-dilute regime, $\rho_b/\rho^* > 1$, we therefore also perform configurational bias Monte Carlo (CBMC) moves [33,34], in which part of the interior polymer is regrown. In addition, we attempt reptation moves where a limited number of segments at one end of the polymer are removed and regrown at the other end. By regrowing the polymer a bias is introduced, which is then corrected for in the sampling [33,34]. In the

simulations at high densities, we find that we can regrow groups of up to about 20-40 segments in a CBMC move with a reasonable acceptance ratio (about 40 - 50 %). More sophisticated algorithms for very dense polymer systems are available [35], but are not necessary in our relatively dilute systems.

III. EFFECTIVE POTENTIALS: TWO ISOLATED POLYMERS

The theory of the effective interaction between two polymer coils in dilute solution has a long history. The first calculations were by Flory and Krigbaum in 1950 [23], who showed that, within a mean-field picture, SAW polymers in a good solvent have a strongly repulsive interaction of the form:

$$\beta v_2^{(FK)}(r) \sim L^2 \left(\frac{3}{4\pi R_g^3} \right) (1 - 2\chi) \exp \left(-\frac{3}{4} \frac{r^2}{R_g^2} \right), \quad (1)$$

where r is the distance between the CM of the two polymer coils, χ is the usual Flory parameter, and $\beta = 1/k_B T$ is the reciprocal temperature, with k_B denoting Boltzmann's constant. As long as the polymers are in a good solvent, the chains can be regarded as athermal, and for that reason we set $\beta = 1$ in the rest of this paper.

The interaction strength at full overlap, $v_2^{(FK)}(r=0)$, can be understood from the following argument: each polymer coil has a density of monomers $c \sim L/V$, while the volume of a polymer scales as $V \propto L^{3\nu}$, so that $c \propto L^{1-3\nu}$ (here $\nu \approx 0.6$ is the Flory exponent). If two polymers overlap completely then the mean-field free-energy of interaction would be proportional to the number of monomers times the probability of contact of two monomers on different chains:

$$v_2^{(FK)}(r=0) \propto Lc \propto L^{2-3\nu} \sim \mathcal{O}(L^{0.2}), \quad (2)$$

which implies that the polymer repulsion increases with polymerization L , and is typically much larger than $k_B T$.

In an elegant paper, Grosberg, Khalatur, and Khokhlov [36] showed that Flory's argument was in fact incorrect. From scaling theory it follows that the probability of an interaction between two monomers on different chains scales as $c^{1/(3\nu-1)} \sim c^{1.3}$ [37] instead of simply c , so that the free energy of interaction scales as:

$$v_2(r=0) \propto Lc^{1/(3\nu-1)} \sim L(L^{1-3\nu})^{1/(3\nu-1)} \sim \mathcal{O}(1). \quad (3)$$

In other words, the free energy of interaction at full overlap of two equal-length polymers is independent of the degree of polymerization; polymer coils are not nearly as "hard" as one might naively expect.

Krüger, Schäfer, and Baumgärtner [38] put these ideas on a firmer footing using elaborate renormalization group (RG) calculations. In particular they calculated the full

free-energy of overlap of polymers as a function of the CM distance. They found $v_2(r=0) = 1.53\epsilon$ from an r -space ϵ expansion and $v_2(r=0) = 0.94\epsilon + 0.62\epsilon^2$ from a k -space ϵ expansion ($\epsilon = 4 - d$, so $\epsilon = 1$ for 3 dimensions). Although there are still significant quantitative differences between an $\mathcal{O}(\epsilon)$ and an $\mathcal{O}(\epsilon^2)$ calculation, implying that the ϵ expansion has not quite converged, the qualitative picture is clearly that of a repulsive Gaussian type potential, as shown in Fig. 2. These calculations were confirmed by a number of computer simulation studies, notably those by Olaj and collaborators [39], and by Dauntenhahn and Hall [30].

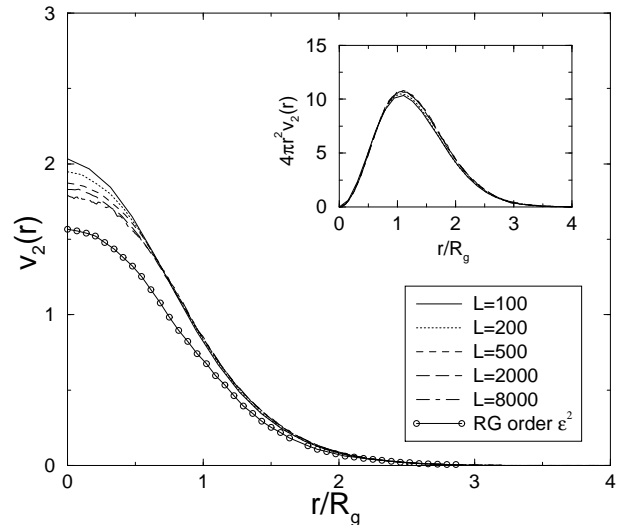


FIG. 2. Effective CM-CM pair potential $v_2(r)$ for two isolated SAW polymers, here shown for different lengths L . The x-axis is scaled with R_g , to allow comparison. The pair interaction $v_2(r)$ is approximately Gaussian. The height of the potential at $r=0$ decreases with length. Also shown is the RG result from an order $\mathcal{O}(\epsilon^2)$ expansion. Inset: $4\pi r^2 v_2(r)$, which is more relevant to the thermodynamics of polymer solutions, shows much less variation with length L than $v_2(r)$.

We repeated the calculation of the effective interaction between two isolated SAW polymer coils, to make sure that the simulations are carried out under conditions sufficiently close to the scaling limit. For two polymers at infinite dilution, the effective interaction can be determined by calculating the normalized probability $P(r)$ of finding their respective CM's at a separation r . The effective potential $v_2(r)$ is then defined as

$$v_2(r) = -\ln(P(r)) \quad (4)$$

In the course of the simulation we sample configurations of two polymers infinitely far apart using only the pivot algorithm. After every 1000 pivot moves, we calculate the overlap probability as a function of CM distance, by moving the polymers towards each other while checking for overlap. In addition, the radius of gyration is calculated for each length considered, from $L = 100$ to

$L = 8000$. This reproduces the well known Flory scaling law $R_g \sim L^\nu$. The effective interactions between two polymers of various lengths are plotted in Fig. 2; the distance r is scaled with the measured radius of gyration R_g . As expected, $v_2(r)$ has a Gaussian shape centered on $r = 0$. The potentials are almost indistinguishable for $r/R_g > 1$, but for smaller r the potentials differ slightly for different L . This is most pronounced at full overlap of the polymers, where $v_2(r = 0)$ decreases with length L . In the scaling limit $L \rightarrow \infty$, $v_2(r = 0)$ is expected to reach a finite value while for finite L , we expect $v_2(r = 0)$ to scale as:

$$v_2(r = 0) \propto L \ln(1 - ac^{1/(3\nu-1)}) \sim L \ln(1 - \frac{a}{L}) \quad (5)$$

where a is a (negative) constant and the logarithmic term arises because $P(r)$ scales linearly. This finite-size scaling behavior is confirmed in Fig. 3 and in the $L \rightarrow \infty$ limit this equation goes over to Eq. (3). Using a non-linear fit of the MC data to Eq. (5) we estimate $v_2(r = 0) = 1.80 \pm 0.05$, a value slightly higher than the best $\mathcal{O}(\epsilon^2)$ RG calculations which give $v_2(r = 0) = 1.53$. The difference is most likely due to a lack of convergence of the ϵ expansion [38].

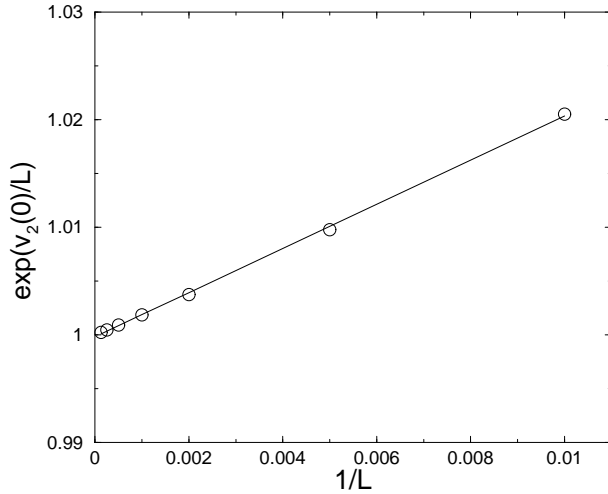


FIG. 3. Finite-size scaling for the interaction between two isolated polymers at full overlap: $v_2(r = 0)$. By plotting $\exp[v_2(r = 0)/L]$ v.s. $1/L$, the agreement between the scaling relation of Eq. (5) and the simulations is demonstrated.

The quantity $r^2 v_2(r)$ is actually more relevant for the thermodynamic properties of polymer solutions than $v_2(r = 0)$ [40], and, as demonstrated in the inset of Fig. 2, the former varies less with L than the latter, such that for $r^2 v_2(r)$ the scaling limit appears to be reached even for chains as short as $L = 500$.

Similarly, with the effective pair-potentials we can calculate the 2nd osmotic virial coefficient:

$$B_2 = -2\pi \int_0^\infty r^2 dr (\exp(-v_2(r)) - 1). \quad (6)$$

Since the potentials scale with r/R_g , this means that B_2/R_g^3 should be independent of L in the scaling limit. As demonstrated in Fig. 4, the scaling limit appears to be practically reached for $L = 500$. We estimate that for $L \rightarrow \infty$, $B_2/R_g^3 \approx 5.85 \pm 0.05$, which is consistent with other results obtained from simulations ($B_2/R_g^3 \approx 5.50$ [41]) or RG calculations ($B_2/R_g^3 \approx 5.99$ [42]). Note that although B_2 scales as $B_2 \sim R_g^3$, as required by scaling theory [1,2,4], this does not imply that the polymer-polymer interaction is hard-sphere like, as is sometimes implied in the literature [43].

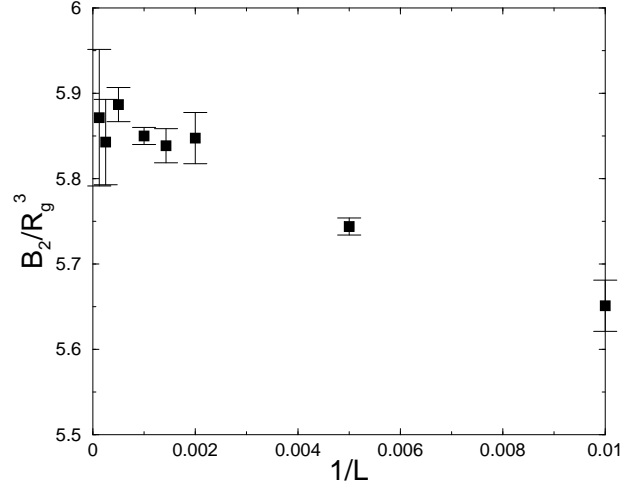


FIG. 4. The reduced osmotic virial coefficient B_2/R_g^3 v.s. $1/L$.

IV. EFFECTIVE POTENTIALS: POLYMER SOLUTIONS

A. Deriving effective potentials from $g(r)$

Having derived the effective potential between two isolated polymers, we now attempt the same for polymers in solution at finite concentration. Whereas for simple fluids, the interaction potential is generally independent of the thermodynamic state, this is not true for effective potentials in complex fluids. The latter typically follow from a coarse-graining procedure, which amounts to averaging out certain degrees of freedom, the individual microscopic polymer segments in the present case. The effective total interaction potential energy $V_N(\{\mathbf{r}_i\}; \rho_b)$ is in fact a *free energy* which depends here on the polymer density $\rho_b = N/V$ and on the configuration $\{\mathbf{r}_i\}$ of the polymer CM's. The bare pair-interaction term $v_2(r)$ can be defined as the effective potential between two isolated polymers, the bare triplet interaction term $v_3(\mathbf{r}_i, \mathbf{r}_j, \mathbf{r}_k)$ can be defined for three isolated polymers and so forth. One could in principle calculate higher and higher order n -body terms, but this rapidly becomes intractable.

Even if explicit expressions for each of the terms were obtained, the total interaction energy would be very difficult to evaluate because the number of n -tuple coordinates increases exponentially.

Instead, we follow a different route and approximate the pair and higher order terms by an effective, (state dependent) pair interaction $v(r; \rho_b)$ which is constructed to exactly reproduce the two-body correlations of the full underlying many-body system. In fact, it can be proven that for any given pair distribution function $g(r)$ and density ρ_b , there exists a corresponding *unique* two-body pair potential $v(r; \rho_b)$ which reproduces $g(r)$ *irrespective of the underlying many-body interactions* in the system [44]. Of course, $g(r)$ will contain contributions not only from the bare pair-potential $v_2(r)$, but also from the three and more body terms. As a consequence, the effective pair interaction $v(r; \rho_b)$ will also be state dependent (in the polymer case, density dependent) and a new effective potential must be calculated for each density. Nevertheless, the effective potential leads back to the true thermodynamics of the full many-body system through the compressibility relation:

$$\left(\frac{\partial \Pi_b}{\partial \rho_b} \right)_{N,T} = \frac{1}{1 - \rho_b \hat{h}(k=0)} = 1 - \rho_b \hat{c}(k=0), \quad (7)$$

where $\hat{h}(k)$ is the Fourier transform (FT) of the pair correlation function $h(r) = g(r) - 1$, and $\hat{c}(k)$ is the FT of the direct correlation function. Using a variational argument, Reatto [45] has shown that $v(r; \rho_b)$ may also be viewed as the “best” pair representation of the true interactions. However this inversion approach says nothing about a possible volume term $V_0(\rho_b)$, in the coarse-grained total potential energy, which contributes to the e.o.s., but not *directly* to the pair-correlations [46]. Of course the volume terms may still contribute *indirectly*, for example when they induce phase-transitions.

The inversion of $g(r)$ to extract $v(r; \rho_b)$ is a well known procedure and has been studied extensively in the field of simple fluids [45,47]. We invert $g(r)$ using the hypernetted-chain (HNC) closure,

$$g(r) = \exp(-v(r) + g(r) - c(r) - 1), \quad (8)$$

of the Ornstein-Zernike equation [48]. While the simple HNC inversion procedure would be inadequate for dense fluids of hard core particles, where more sophisticated closures or iterative procedures are required [45,47], we are able to demonstrate the consistency of the HNC inversion in the present case.

We performed Monte Carlo simulations of N SAW polymers of length $L = 500$ on a cubic lattice of size $M = 240 \times 240 \times 240$. The number of polymers was varied from $N = 100$ ($\rho_b/\rho^* = 0.54$) to $N = 6400$ ($\rho_b/\rho^* = 8.7$). Note that at the highest density the monomer packing fraction is $c \approx 0.23$, meaning that the conditions for the

semi-dilute regime, namely $\rho_b > \rho^*$ and $c \approx 0$ begin to be violated. At even higher densities the system will approach the melt regime where monomer packing effects become important [49]. More generally, for finite length SAW polymers, there is a limited density regime for which both conditions for the semi-dilute regime can be simultaneously satisfied. We find empirically that $R_g \approx 0.39L^{0.6}$ for SAW polymers on a simple cubic lattice, so that the monomer packing fraction at the overlap concentration is given by

$$c^* \approx 4/L^{0.8}. \quad (9)$$

Thus, for $L = 100$ chains we find $c^* \approx 0.1$ so that there is only a very small density range which might be called semi-dilute, while for $L = 500$ chains $c^* \approx 0.027$ and a meaningful semi-dilute regime exists. The literature contains several claims of semi-dilute scaling behavior for SAW lattice polymers with $L < 100$, but, as the analysis above shows, these polymers do not have a semi-dilute regime large enough to derive scaling relations. An example of this is shown in Fig. 5.

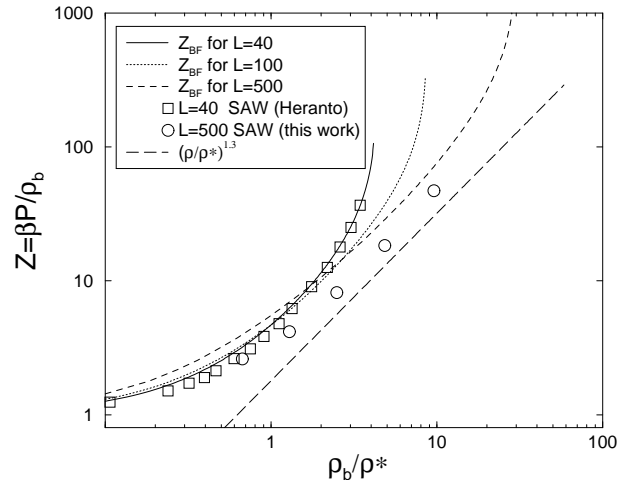


FIG. 5. This figure compares the e.o.s. $Z = \Pi_b / \rho_b$ from simulations for $L = 40$ SAW polymers [50], with the e.o.s. for $L = 500$ SAW polymers (see section IV B), and with the Bawendi-Freed (BF) e.o.s. for lattice models [51], which is accurate for larger values of c . The latter gives an indication where finite c correlations become important, and where one would expect the melt-regime to start for $L = 40$, $L = 100$, and $L = 500$ SAW polymers. In the melt regime the des Cloizeaux scaling law $Z \sim (\rho_b/\rho^*)^{1/(3\nu-1)}$ will break down [6]. Clearly, the $L = 40$ data does not follow the des Cloizeaux scaling law, demonstrating that there is no meaningful semi-dilute regime for $L = 40$ polymers, whereas there is one for $L = 500$ polymers.

In the course of the simulations the CM of each polymer was tracked in order to construct the CM radial pair distribution function $g(r)$. The latter is only known up to a cutoff radius r_c , which corresponds to half the size of the simulation box (lattice size). For the inversion,

we need $g(r)$ for all r , so we employ the following iterative scheme to extend $g(r)$. First we set $g(r) = 1$ for $r > r_c$ and calculate the corresponding $v(r; \rho_b)$ by inversion. We then set $v(r; \rho_b) = 0$ for $r > r_c$ and determine the corresponding $g(r)$ for $0 < r < \infty$ by a regular HNC calculation, using a simple iterative procedure. The $g(r)$ for $r < r_c$ is then replaced by the measured $g(r)$, and the process is repeated until convergence. For low density, $g(r)$ and $v(r; \rho_b)$ converge very quickly, but for higher densities, say $\rho_b/\rho^* > 1$, the convergence is slower, and the mixing factor of the old solution into the new one has to be increased to a value as large as 99%. In fact, because of the finite box-size, the inversion process is underdetermined, and our ansatz that $v(r; \rho_b) = 0$ for $r > r_c$ is needed to find a unique solution. This is not unreasonable since we don't expect the interactions between the polymer coils to be significant beyond a distance a few times the radius of gyration. However, to make sure that this is actually the case, we found that relatively large simulation boxes were needed, with a lattice size of up to $10 - 15R_g$. This is especially important at high density, where the inverted potential becomes longer ranged and more sensitive to small changes in the radial distribution function $g(r)$. In all our inversions we checked explicitly that $v(r; \rho_b)$ becomes effectively zero for an $r < r_c$, confirming our initial ansatz.

The resulting radial distribution functions $g(r)$ are shown in Fig. 6, and are similar in shape to those of the pure Gaussian core model [40]. As the density goes up the correlation hole at small r decreases in range and height. Except for a small maximum around $r \approx 2R_g$, the pair correlation functions do not show oscillations within the statistical noise of about 0.1%, for any density considered here.

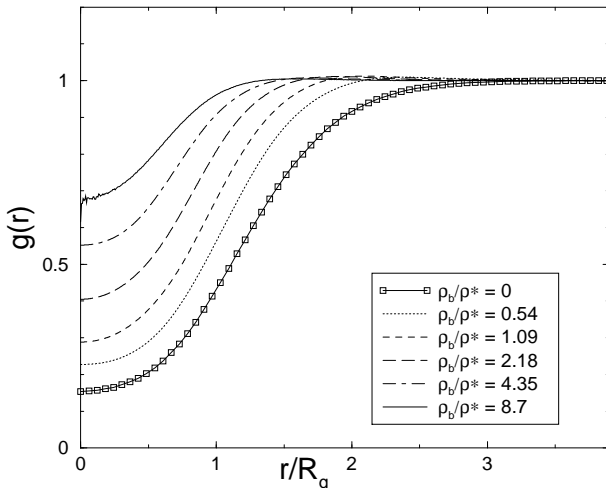


FIG. 6. The polymer CM pair distribution function $g(r)$ calculated for $L=500$ SAW polymers and used to generate $v(r; \rho_b)$. The x-axis denotes r/R_g , where R_g is the radius of gyration of an isolated SAW polymer.

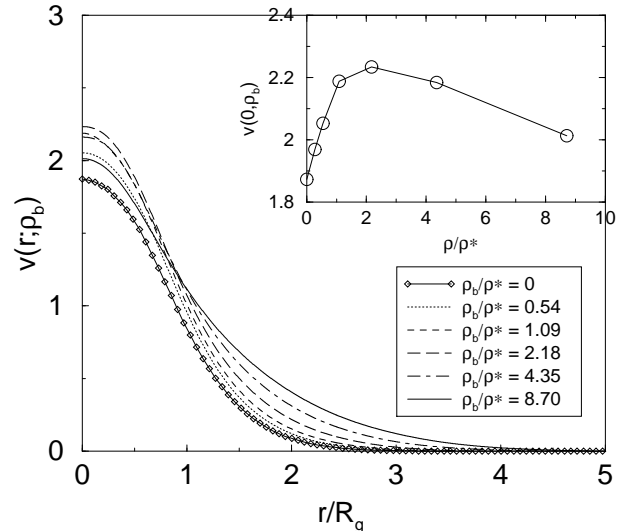


FIG. 7. The effective polymer CM pair potential $v(r; \rho_b)$ derived from an HNC inversion of $g(r)$ for different densities. The x-axis denotes r/R_g , where R_g is the radius of gyration of an isolated SAW polymer. Inset: The value of the effective polymer CM pair potential at $r = 0$, as a function of density ρ_b/ρ^* . The maximum of the potential initially increases before decreasing at high concentration.

The effective polymer-polymer potentials $v(r; \rho_b)$, obtained from the $g(r)$'s, are shown in Fig. 7. Careful inspection of the figure reveals that the effective pair potential is not very sensitive to the polymer concentration. The value at $r = 0$ first increases slightly with ρ_b , before decreasing again at the highest concentrations, as is depicted in the inset of Fig 7, while the range of $v(r; \rho_b)$ increases with ρ_b . A more subtle feature, highlighted in Fig. 8, is that the effective potential becomes slightly negative ($\mathcal{O}(10^{-3}k_B T)$) for $r/R_g \gtrsim 3$ at the higher concentrations. These effects become apparent only when large enough box-sizes are used. Although the negative tails seem very small, they are nevertheless significant since the thermodynamics depend on the integral of $r^2 v(r; \rho_b)$. For example, leaving them out can easily induce a 5% change in the pressure. It is, therefore, paramount to include these effects in (quasi)-analytical representations of the effective potentials. For that reason, a simple fit to a Gaussian or a sum of Gaussians is not accurate enough to reproduce the structure and the thermodynamics of the SAW polymer systems and consequently, we chose to use an interpolation spline fit to describe the potentials. First, the raw effective potential data were fitted to a Gaussian:

$$v_{\text{est}}(r) = a_0 e^{-a_1 r^2}. \quad (10)$$

Subsequently, the difference $\Delta v(r; \rho_b) = v(r; \rho_b) - v_{\text{est}}(r)$ was fitted by employing a least squares spline procedure with 8 nodes (the “dfc” routine of the slatec library [52]). The values of the nodes are not known in

advance, except for the boundaries $r = 0$ and $r = r_c$. Additional constraints on the spline fit were: $v(r_c) = 0$, $dv(r = r_c)/dr = 0$ and $v(r = 0)/dr = 0$. We optimized the spline fit by moving the nodes on the x-axis using a Monte Carlo procedure. The parameters for the fits are available elsewhere [53].

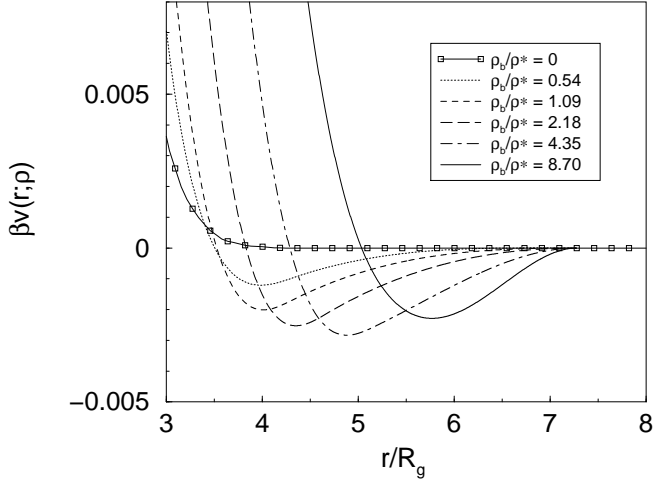


FIG. 8. The negative part of the effective polymer CM pair potential $v(r; \rho_b)$ derived from an HNC inversion of $g(r)$ for different densities. The x-axis denotes r/R_g , where R_g is the radius of gyration of an isolated SAW polymer.

Note that in Fig. 7, the polymer-polymer interaction $v(r; \rho_b)$ is plotted v.s. r/R_g , where R_g is the radius of gyration of *isolated* polymers in the infinitely dilute limit. In a dense solution, the effective radius of gyration of the polymers contracts according to the power-law, $R_g \sim \rho_b^{-1/8}$ [2,37,54], as shown in Fig. 9.

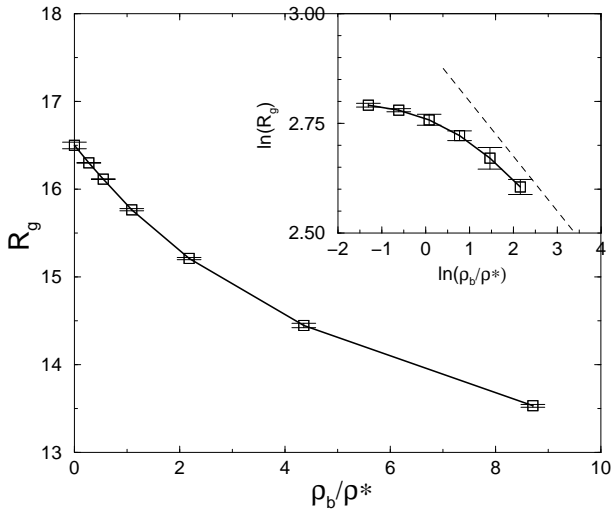


FIG. 9. The effective radius of gyration for $L = 500$ SAW polymers decreases as a function of density ρ_b/ρ^* . **Inset:** At high densities the effective radius of gyration asymptotically follows the scaling law $R_g \sim \rho_b^{-1/8}$.

The accuracy of the effective potentials are tested by performing a direct Molecular Dynamics (MD) simulation of the “soft colloids” interacting via $v(r; \rho_b)$. In Fig. 10 the pair distribution function $g_{\text{MD}}(r)$ from MD simulations is compared with the original SAW $g(r)$ for two densities in the semi-dilute regime. The difference between the two distribution functions shows an oscillation at small r . Because this occurs in the same way for both densities it is possibly introduced by the inversion procedure. Even so, the difference between the two distribution functions is still typically less than ± 0.01 . We conclude that the HNC inversion procedure yields very accurate effective potentials for soft particles, capable of describing the structure of the fluid with an absolute error of less than ± 0.01 .

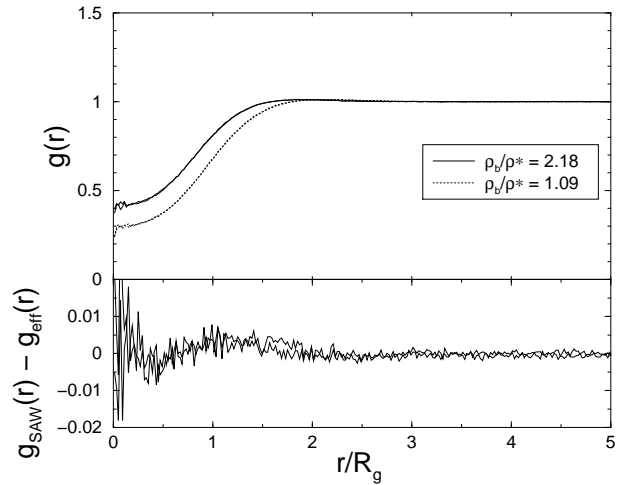


FIG. 10. The $g(r)$ of a system interacting via the effective potential $v(r; \rho_b)$ compared with the CM pair distribution of a SAW simulation for two polymer concentrations. The differences are shown in the lower panel and are typically less than ± 0.01 .

In a previous paper we have shown that the HNC closure is very accurate when applied to the Gaussian model [55], whereby particles interact via the repulsive potential $v(r) = \epsilon \exp[-\alpha (r/R_g)^2]$, and is in fact quasi-exact in the regime relevant to the effective potentials shown in Fig. 7 [40,56]. Even the much cruder RPA closure, $c(r) = -v(r)$, yields semi-quantitatively accurate results for correlations and thermodynamics in the regime of interest. Thus polymer solutions in the dilute or semi-dilute regime fall into the class of mean field fluids according to the nomenclature introduced in Ref. [40].

The inversion procedure guarantees that the two-body correlations are accurately reproduced by the effective potential, but this does not necessarily imply that higher order correlations are also well represented. As a first test we performed preliminary simulations of the three-body bond-order correlation functions $g_3(r, \theta, \varphi)$ for both full SAW walks and our soft particles. The two approaches

lead to identical results within statistical errors, implying that higher order correlations are much more accurately reproduced than one might initially expect. We have also performed some preliminary calculations of the three-body interaction $v_3(\mathbf{r}_1, \mathbf{r}_2, \mathbf{r}_3)$. Even at full overlap of the three centers of mass, the three-body interaction term is only about 10% of the pairwise interaction. This is consistent with the results found for star-polymers [57], and was fore-shadowed by the relatively weak density dependence of the effective pair interaction $v(r; \rho_b)$.

Besides accurately describing the structure, it is also important that the thermodynamics are captured by the effective potential. In the next section we therefore focus on the equation of state (e.o.s.) for polymer solutions.

B. Equation of state

1. Equation of state from direct SAW simulations

We measured the e.o.s., Π_b/ρ_b , directly for a SAW simulation by using the thermodynamic integration approach of Dickman [58]. In this method the bulk (osmotic) pressure Π_b is measured by taking the derivative of the free energy F with respect to volume of a system of SAW polymers between two hard walls. The polymers live on a rectangular cubic lattice of size $M = H \times D \times D$, which is periodic in the y and z directions. The two walls are represented by an infinitely repulsive potential at $x = 0$ and at $x = H + 1$, so that the polymer segments cannot penetrate the walls. The volume of a lattice can only change discretely, and the free energy derivative changes to a finite difference

$$\Pi_b = \frac{\partial \ln Z(N, L, D, H)}{\partial M} = D^{-2} \frac{\partial \ln Z(N, L, D, H)}{\partial H} \approx D^{-2} (\ln Z(N, L, D, H) - \ln Z(N, L, D, H-1)). \quad (11)$$

The model is modified by associating an additional repulsive potential $-\ln \lambda$ with each occupied site in the plane $x = H$, where $0 < \lambda < 1$. The partition function then becomes

$$Z(N, L, D, H\lambda) = \sum_{\text{polymer conf}} e^{-U} \cdot \lambda^{n_H}, \quad (12)$$

where $n_H = D^2 \rho_H(\lambda)$ is the number of occupied sites in the $x = H$ plane, and $\rho_H(\lambda)$ is the corresponding number density in this plane. The pressure can now be estimated as

$$\Pi_b = D^{-2} \int_0^1 d\lambda \left(\frac{\partial \ln Z}{\partial \lambda} \right) = \int_0^1 d\lambda \frac{\rho_H(\lambda)}{\lambda} \quad (13)$$

We performed SAW simulations of polymers with length $L = 500$ on a $M = 160 \times 100 \times 100$ cubic lattice for $N = 50, 100, 200, 400, 600$ and 800 . For each density we

determined the value of $\rho_H(\lambda)$ for 5 different values of λ , corresponding to the abscissae of a 5 point Gaussian quadrature which was used to evaluate the integral in Eq. (13). The resulting e.o.s. is plotted in Fig. 11.

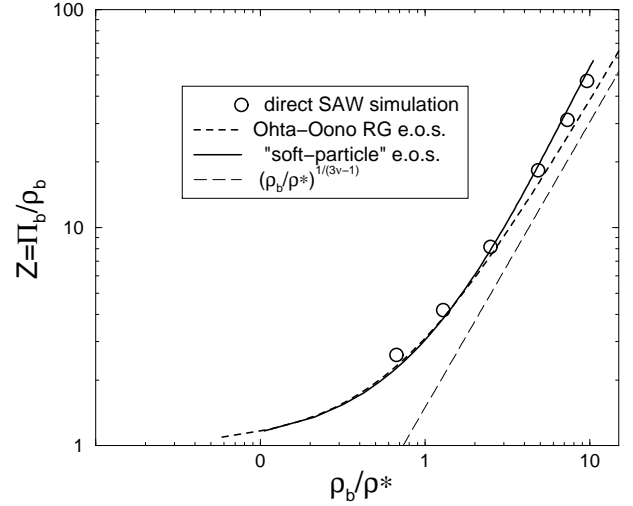


FIG. 11. Log-log plot of the e.o.s. $Z = \Pi/\rho_b$ as a function of the density for $L = 500$ polymers. The soft-particle e.o.s. gives a good representation of the full SAW polymer simulations. At the highest densities there is a slight deviation from the expected des Cloizeaux $(\rho_b/\rho^*)^{1/(3\nu-1)}$ scaling law which we attribute to the effects of a finite monomer concentration c . Also shown is the RG e.o.s. of Ohta and Oono [60,61].

2. Equation of state from the soft-particle picture

To calculate the e.o.s. within the soft-particle picture, we use the compressibility relation (7), which must now be integrated w.r.t. the density:

$$\Pi_b(\rho_b) = \int_0^{\rho_b} (1 - \rho' \hat{c}(0, \rho')) d\rho'. \quad (14)$$

We used the quasi-exact HNC approximation to calculate $c(r)$ from the inverted effective potential $v(r; \rho_b)$ for several state-points, fitted the values of $\hat{c}(0; \rho_b)$, and integrated w.r.t. density. As demonstrated in Fig. 11, the e.o.s. is very close to the one obtained by direct SAW simulations, immediately suggesting that our inversion procedure indeed reproduces the true thermodynamics of the full many-body system. This success also implies that the volume terms are small, possibly smaller than the statistical error in our present simulations and inverted potentials. In fact, using a simple scaling theory, Likos has argued that the contribution of volume terms to the e.o.s. scales as $(\rho_b/\rho^*)^{3/8}$ in the semi-dilute regime, and so contributes little to the full e.o.s. [59].

Also shown in Fig. 11 is the RG result by Ohta and Oono [60]; we use a slight improvement with correct exponents [61]. The one remaining fit parameter is determined by the second osmotic virial coefficient B_2 for

$L = 500$ SAW polymers, a procedure similar to that used when comparing to experiment [62]. The agreement is seen to be fairly good, although the SAW e.o.s. is somewhat higher than the RG results. This is most likely due to the fact that the monomer density c is not zero, which induces small corrections to the full scaling limit (see the discussion in Section IV A).

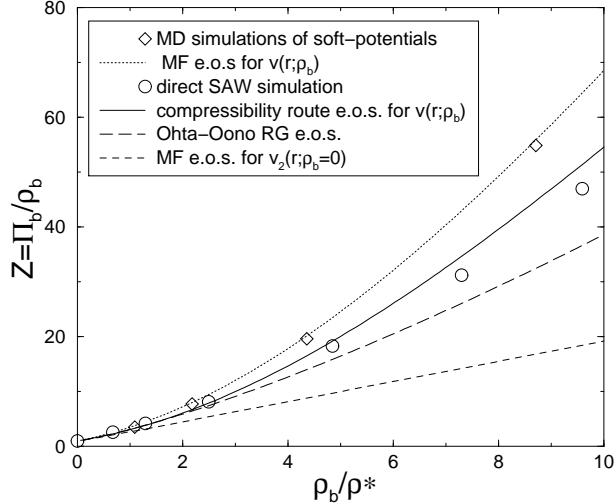


FIG. 12. Linear plot of the the e.o.s. $Z = \Pi_b/\rho_b$ as a function of the density for $L = 500$ polymers. Several approximations to the e.o.s., discussed in the text, are compared.

Instead of the compressibility route, one could also use the virial route to the e.o.s. [48]:

$$\frac{\Pi_b}{\rho_b} = 1 + \frac{dV_0(\rho_b)}{d\rho_b} - \frac{1}{3} \sum_{i < j}^N \left\langle r_{ij} \frac{\partial v(r_{ij}; \rho_b)}{\partial r_{ij}} - 3\rho_b \frac{\partial v(r_{ij}; \rho_b)}{\partial \rho_b} \right\rangle, \quad (15)$$

which includes not only the density dependence of the effective pair potential, but also the density dependence of the volume term. The full density dependence of the potentials is at present hard to calculate, so instead we initially ignore the density derivative and the volume terms. First, we directly measured the e.o.s. of the soft-particle fluid by a MD simulation with the spline-fit potentials. The pressure follows from the usual virial theorem, when the density derivatives in Eq. (15) are neglected. The e.o.s. from this approach is depicted in Fig. 12, and compared to the simple mean-field (MF) form:

$$Z_{MF} = 1 + \frac{1}{2} \hat{v}(0; \rho_b) \rho, \quad (16)$$

which gives a good fit to the simulations, as expected for soft-core fluids in the MFF regime [40]. Here $\hat{v}(0; \rho_b)$ is the $k = 0$ component of the FT of the pair interaction. However, by including only the explicit density dependence of the effective pair potentials while ignoring the

density derivative terms in the virial equation, we *overestimate* the e.o.s. compared to the full SAW simulation.

The density dependence can be neglected even further by simply taking the $\rho_b \rightarrow 0$ form of the pair potential, $v_2(r)$, and applying it at all densities. The resulting e.o.s. now *underestimates* the e.o.s. when compared to the full SAW simulation, as demonstrated in Fig. 12. We note that a similar approach was employed in recent work on the phase-behavior of star-polymers, where the $\rho_b \rightarrow 0$ limit of the pair potential was used to calculate the structure and phase-behavior at finite concentration [63].

Finally, we comment on the common practice of extracting osmotic virial coefficients from the measured experimental e.o.s. Firstly, the virial equation has a very small radius of convergence for soft-core fluids [40]. Secondly, the range of the effective potential $v(r; \rho_b)$ increases with density. These two effects imply that a naive linear fit to all but the very lowest polymer densities will lead to an overestimate of the true osmotic second virial coefficient B_2 .

V. EFFECTIVE WALL-POLYMER POTENTIALS

A. Polymer coils near a wall

Polymer coils near a non-adsorbing hard wall exhibit a depletion layer due to entropic effects. This is true even for ideal Gaussian polymers, and if one were to model these by effective CM potentials, the polymer-polymer potential would be zero, but there would still be a polymer-wall potential of the form $\phi(z) = \ln(\rho(z)/\rho_b)$, where $\rho(z)$ is the CM density profile near the wall and ρ_b is the uniform density far from the wall (see the Appendix for more details). Thus a complete description of polymer coils in confined geometries requires not only the polymer-polymer interactions derived in the previous section, but also effective polymer-wall potentials $\phi(z; \rho_b)$.

We follow a strategy similar to that used in the homogeneous case, and first calculate the wall-polymer density profile $\rho(z)$, from which we then extract an effective potential $\phi(z; \rho_b)$. Using the same explicit SAW polymer model as in Section II, we performed MC simulations of polymers of length $L = 500$ on a lattice of size $M = 160 \times 100 \times 100$ with hard walls at $x = 0$ and $x = 160$. The polymer segments were not allowed to penetrate the walls. The simulations were done for $N = 50, 100, 200$ and 500 . During each simulation, we computed the density profiles $\rho(z)$, where z denotes the distance of the polymer CM from the wall and ρ_b is the bulk density far from the wall. The normalized profiles $h(z) = \rho(z)/\rho_b - 1$, for different bulk concentrations ρ_b/ρ^* are shown in Fig. 13.

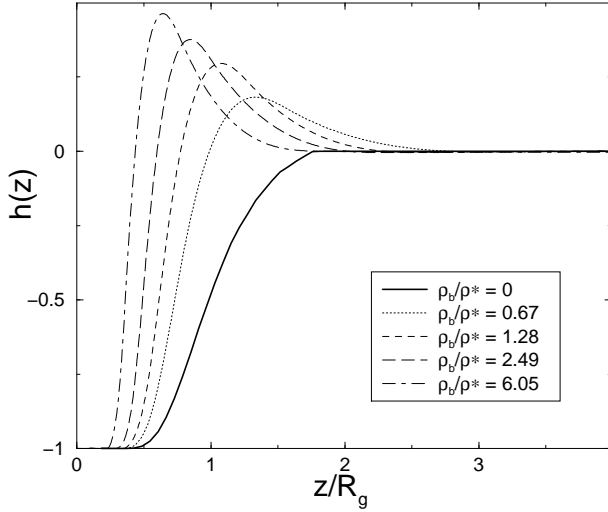


FIG. 13. The wall-polymer CM density profile $h(z) = \rho(z)/\rho_b - 1$ for SAW polymers at different bulk concentrations. From $h(z)$ we can calculate the corresponding polymer adsorptions Γ and find $-\Gamma = 0, 0.094, 0.13, 0.16$, and 0.20 in units of R_g^{-2} respectively. The relative adsorptions are $-\Gamma/\rho_b = 0.84, 0.59, 0.41, 0.27$, and 0.14 respectively, and decrease with increasing density as expected.

The polymer coil adsorption Γ is defined by:

$$\Gamma = -\frac{\partial(\Omega^{ex}/A)}{\partial\mu} = \rho_b \int_0^\infty h(z) dz, \quad (17)$$

where Ω^{ex}/A is the excess grand potential per unit area and μ the chemical potential of the polymers. As the density increases, more polymer is adsorbed at the wall as expected, but the relative adsorption, Γ/ρ_b , decreases.

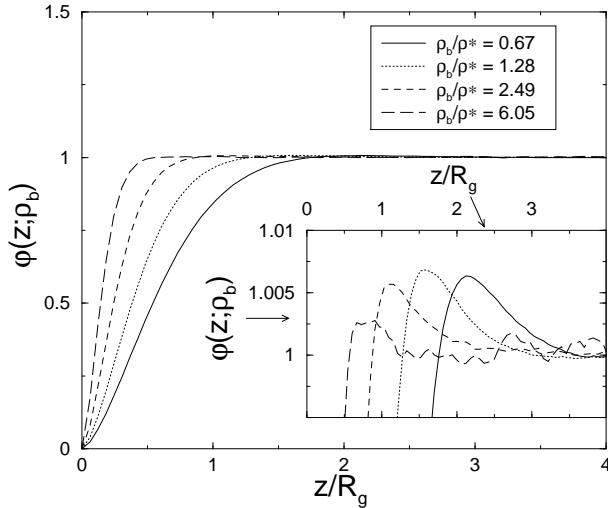


FIG. 14. The wall-monomer density profile $\varphi(z; \rho_b) = \rho(z)/\rho_b - 1$ for the same set of densities as in Fig.13. **Inset:** A magnification of the region where there is a small correlational bump in the density profiles. The height is less than 1% of the total density while the range is about R_g , implying that the bump arises from polymer-polymer correlations.

The normalized monomer density profiles for SAW's are shown in Fig. 14 for the same polymer densities as the CM profiles shown in Fig. 13. As expected, the profile moves closer to the wall for higher density; the width of the monomer depletion layer shifts from around R_g at the lowest densities, down to values dictated by the segment correlation length [2] in the semi-dilute regime. Although the profiles do not show such a clear correlation-induced oscillation as the CM profiles, there is nevertheless still a small maximum in the depletion layer as illustrated in the inset of Fig 14. The peak in the monomer profile is less than 1% of the bulk density, and seems to decrease for higher overall polymer concentration. The range is about R_g , implying that it arises from correlations between polymer coils. We observe only one peak, although due to statistical noise, we cannot rule out the possibility of more oscillations in the density profiles. Recently self-consistent field calculations, valid for polymers in a theta solvent, found a similar small oscillation in the monomer profiles [64].

B. Deriving $\phi(z; \rho_b)$ from $\rho(z)$

From a knowledge of the concentration profile $\rho(z)$, and the bulk direct correlation function between polymer CM's, $c_b(r)$, one may extract an effective wall-polymer potential $\phi(z; \rho_b)$ by combining the wall-polymer OZ relations [48] with the HNC closure. For a binary mixture of two components labeled 0 and 1, in which component 0 is infinitely dilute ($x_0 \rightarrow 0$), the Ornstein-Zernike equations become [48]

$$h_{11}(1, 2) = c_{11}(1, 2) + \rho_b \int h_{11}(1, 3) c_{11}(2, 3) d3 \quad (18a)$$

$$h_{10}(1, 2) = c_{10}(1, 2) + \rho_b \int h_{11}(1, 3) c_{10}(2, 3) d3 \quad (18b)$$

$$h_{01}(1, 2) = c_{01}(1, 2) + \rho_b \int h_{01}(1, 3) c_{11}(2, 3) d3 \quad (18c)$$

$$h_{00}(1, 2) = c_{00}(1, 2) + \rho_b \int h_{01}(1, 3) c_{10}(2, 3) d3 \quad (18d)$$

In the limit $R_0 \rightarrow \infty$, Eq. (18c) becomes an equation for the wall-density profile, sometimes called the wall-OZ relation:

$$h(z) = c_{01}(z) + \rho_b \int d\mathbf{r}' h_{01}(z') c_b(|\mathbf{r} - \mathbf{r}'|), \quad (19)$$

where $h(z) = \rho(z)/\rho_b - 1$. The wall-OZ equation can be solved, given the bulk correlation function $c_b(r)$, and a closure relation. In Section. IV A we showed that the HNC closure gives excellent results for effective polymer-polymer interactions, and it is therefore natural to apply

the same approximation here. Combining Eq. (8) with Eq. (19) we obtain

$$\phi(z; \rho_b) = \phi^{MF}(z; \rho_b) + \rho_b \int d\mathbf{r}' h(z') c_b(|\mathbf{r} - \mathbf{r}'|). \quad (20)$$

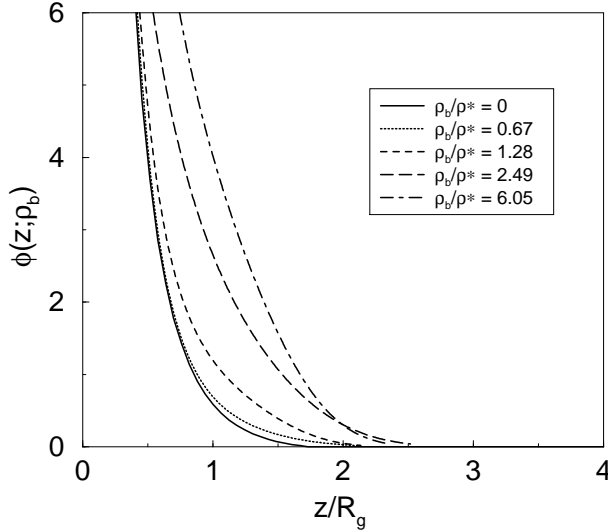


FIG. 15. The wall-polymer potential $\phi(z; \rho_b)$ as obtained from the inversion of $h(z)$ via the HNC expression, Eq. (20).

The first term is the usual potential of mean force $\phi^{MF}(z; \rho_b) = -\ln[\rho(z)/\rho_b]$, to which $\phi(z; \rho_b)$ would reduce in the $\rho_b \rightarrow 0$ limit, while the second term arises from correlations between the polymer coils next to the wall. An identical equation results from the HNC density functional theory (DFT) approach [65], and a similar one, with $c_b(r)$ replaced by $v(r; \rho_b)$ obtains if a mean field DFT is used. In contrast to simple fluids, where Eq. (20) is not very reliable, the wall-HNC closure works remarkably well for the Gaussian core-fluid in the regime relevant to polymer solutions [40]. Using the $c_b(r)$ extracted from the earlier bulk simulations of $g(r)$ (see Section IV A), together with Eq. (20), we are able to extract $\phi(z; \rho_b)$ from the density profiles. In order to calculate the integral in Eq. (20), we use the procedure outlined by Sullivan and Stell [66]. In contrast to the inversion of the bulk $g(r)$, where we had to iterate until convergence, the wall-polymer inversion requires only one step since $c_b(r)$ is given once and for all. Results for various bulk concentrations are plotted in Fig. 15. The range of the effective wall-polymer repulsion increases with increasing concentration, while the density profiles actually move in closer to the wall. The compression and enhanced correlation in the density profiles with increasing density resembles that of the pure Gaussian core fluid in a fixed external potential [40], but the effect is less pronounced in the former case since for polymer solutions the wall-polymer potential becomes more repulsive with density. This is

due mainly to the correlation term, which is nearly linear in ρ_b , and so becomes relatively more important as the density increases. Nevertheless at shorter distances the $\phi^{MF}(z; \rho_b)$ term still dominates. The importance of including both the potential of mean force, and the correlation-induced component of the effective potential is demonstrated in Fig. 16. At very low densities the potential of mean force is adequate, but at higher densities the correlation term becomes increasingly important.

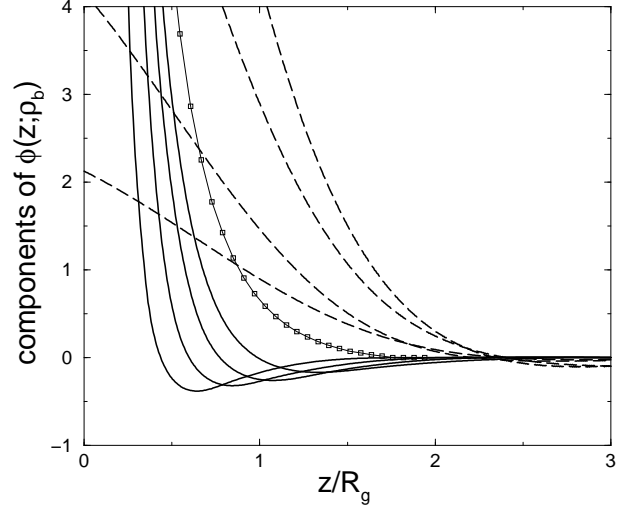


FIG. 16. Comparison between the contributions to the effective wall-polymer potentials from the potential of mean force (solid lines) and from the correlation part (dashed lines) (cf. Eq. (20)) for polymer concentrations $\rho_b/\rho^* = 0.67, 1.28, 2.49$ and 6.05 . From top to bottom the solid lines correspond to increasing density and the dashed lines correspond to decreasing density. The solid line with the small squares denotes the potential of mean force for infinitely diluted systems.

The effective potentials decay exponentially, and to obtain a useful analytic form for the effective potential, the logarithm of $\phi(z; \rho_b)$ can be fitted to a cubic polynomial, which describes the potential very well. However, as in the bulk case, the wall-polymer potential $\phi(z; \rho_b)$ has a small negative component that cannot be described by an exponential function. Although in this case the tail is probably not very important, in order to be consistent, we fit $\phi(z; \rho_b)$ by a least squares spline fit similar to the one described Section. IV A. The parameters for this fit are available elsewhere [53].

C. Consistency of the wall-polymer inversion

To test the validity of the inversion procedure for the wall-polymer $\rho(z)$, we performed Molecular Dynamics simulations of a system of “soft colloidal” particles interacting with each other via the effective pair potential $v(r, \rho_b)$ and with a wall via the inverted potential $\phi(z; \rho_b)$

for the appropriate bulk concentration ρ_b . Such effective potential simulations are at least an order of magnitude faster than simulations of the original SAW model. The resulting concentration profile of the effective particles is shown in Fig. 17 for one density; it agrees to within an absolute error of roughly ± 0.02 with the $\rho(z)/\rho_b$ obtained from the detailed SAW simulations. The corresponding adsorption Γ also differs by less than 1% from the value obtained by the SAW simulation, thus demonstrating the adequacy of the soft colloid representation of the interacting polymer coils, and the accuracy of the HNC inversion for polymer coils near a hard wall.

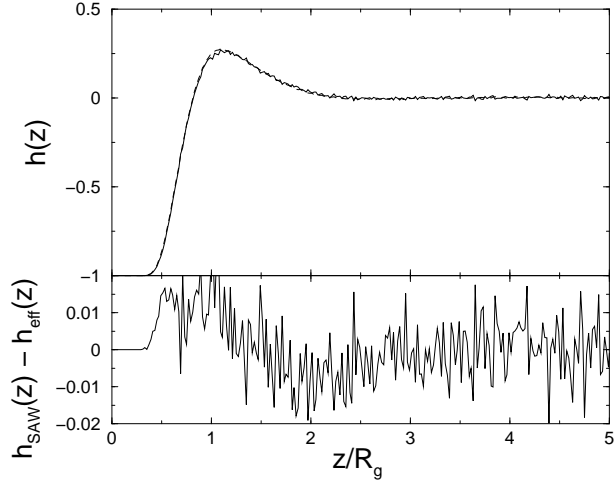


FIG. 17. The profile $h(z)$ of a system of soft colloids near a wall (dashed line). The particles interact with each other via $v(r)$, and with the wall via $\phi(z; \rho_b)$. This is compared with the wall-CM distribution of an explicit SAW simulation (solid line). The difference is shown in the lower panel and is less than ± 0.02 .

VI. DEPLETION POTENTIAL BETWEEN TWO WALLS

A. Full SAW simulations

One of the aims of this work is to show that the soft particle description of the polymers provides a useful route to the colloid-colloid depletion potential in mixtures of colloidal particles and non-adsorbing polymers. Calculating these depletion interactions poses a severe test of the soft colloid representation.

As a first step we calculate the depletion potential between two planar walls, which can ultimately be applied to spherical colloids through the Derjaguin approximation. We confined the polymers within a slit of width d , and, using direct grand-canonical simulations of the full SAW polymer model, we computed the osmotic pressure exerted by the polymer coils on the walls. The insertion of polymers was achieved by the configurational

bias Monte Carlo technique [33]. The (osmotic) pressure $\Pi(d)$ was calculated for different values of the spacing d between the walls by a thermodynamic integration technique similar to the one explained in Section IV B. Details of these simulations can be found in Ref. [67]. The interaction free energy per unit area A , $\Delta F/A$, is then obtained by integrating the osmotic pressure as a function of d :

$$\Delta F(d)/A = \int_d^\infty dz (\Pi(z) - \Pi(\infty)), \quad (21)$$

where $\Pi(\infty)$ denotes the bulk osmotic pressure Π_b . These explicit SAW simulations are rather computer intensive, and were only carried out for $L = 100$ [67].

B. Effective potential simulations

In the soft colloid picture, the interactions of the polymer CM's with each other, $v(r; \rho_b)$, and with a wall, $\phi(z; \rho_b)$, are calculated once with the HNC inversion procedures from the $g(r)$ and $\rho(z)$ of a full SAW polymer simulation at the bulk density ρ_b . These potentials are then used in grand-canonical MC simulations of soft particles between two walls. The imposed chemical potential is chosen such that for infinitely separated walls the bulk density is recovered. The (osmotic) virial pressure is measured as a function of wall separation d , and the interaction free energy per unit area $\Delta F/A$, is again obtained by integration of the pressure via Eq. (21).

In Fig. 18 the soft colloid depletion interaction is compared to that of the “exact” grand-canonical MC simulations of $L = 100$ SAW polymers, for three different densities, $\rho_b/\rho^* = 0.28, 0.58$ and 0.95 . The two approaches are in good agreement, but the soft colloid calculations are at least two orders of magnitude faster than the SAW simulations. As expected, the depth of the potential increases, whereas the range of the interaction decreases as the density increases [68]. At the two lowest densities, the two approaches agree very well, but for $\rho_b/\rho^* = 0.95$ they differ slightly around $z = 2R_g$ where the soft particle picture shows a larger repulsive barrier. The barrier height is, however, small compared to the attractive minimum at contact, which agrees well with the “exact” data, as does the slope of the attraction.

Liquid state theories for fluids with repulsive particle-particle interactions predict a repulsive barrier [69], so it is not surprising that the soft particle picture shows a small repulsive barrier as well. Instead, it is the lack of a significant barrier for the pure SAW polymer simulations which requires explanation. We trace this effect to the breakdown of the “potential overlap approximation” (POA) described in the Appendix. Under close confinement, the interaction of the soft particles with two parallel walls a distance d apart can no longer be written as the sum of the two individual wall-particle interactions

as would be the case for simple liquids. This is caused mainly by the deformation of the polymers due to the two walls, and also holds for ideal polymers. The failure of the POA can be clearly seen in Fig. 19, where we compare the pressure (or force) profiles for the SAW calculations and the effective potentials. In the soft particle picture the pressure starts to rise at a larger inter-wall distance than the pressure for the SAW polymers, an effect also seen when non-interaction polymers are represented by an effective particle representation based on the CM (see the Appendix). Note that the over and under-estimates of the pressure cancel each other, so that the free energy at contact, $\Delta F(0)$, for the effective potentials is in good agreement with the SAW calculations.

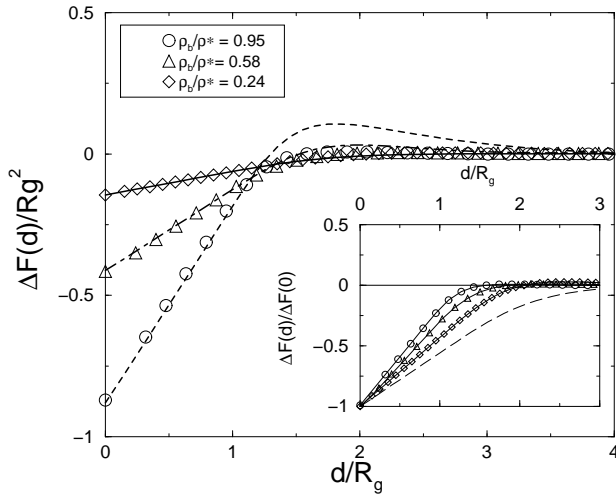


FIG. 18. Depletion free-energy $\Delta F(d)/R_g^2$ between two plates separated by d , for three densities, $\rho_b/\rho^* = 0.95$, $\rho_b/\rho^* = 0.58$, $\rho_b/\rho^* = 0.24$. The symbols denote the “exact” MC simulations, while the dashed, dash-dotted and solid lines are the soft-colloid simulations for the same densities. Inset: $\Delta F(d)/\Delta F(0)$ for the SAW simulations, the solid lines are to guide the eye. The long-dashed line is the ideal Gaussian polymer result calculated in the Appendix. Note that the range decreases with density, and that, even for the lowest density, the AO ideal polymer approximation overestimates the interaction range.

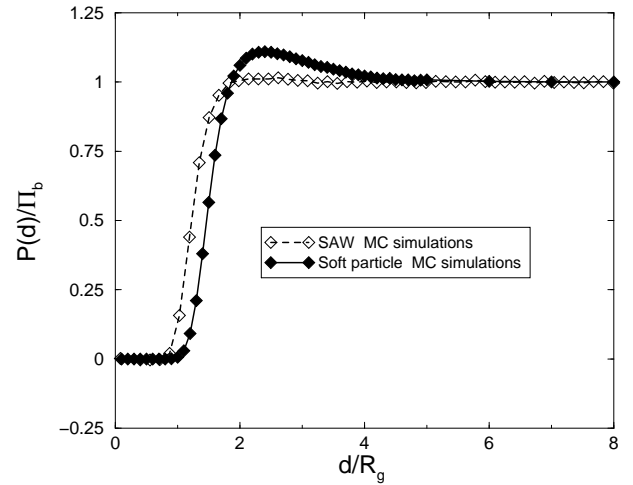


FIG. 19. Comparison of normalized the depletion force per unit area (pressure) $P(d)/\Pi_b$ for SAW polymers and soft particles between two plates separated by d for a density $\rho_b/\rho^* = 0.95$.

The MC simulations for the soft colloid model were carried out with effective wall-polymer and polymer-polymer potentials appropriate for $L = 100$, since longer polymers are not easily handled in the full SAW model. However, we checked that the data obtained with effective interactions appropriate for longer polymers ($L = 500$), are very close to the $L = 100$ results, as is shown in Fig. 20. Therefore, we are confident that we are close enough to the scaling regime for the properties under consideration.

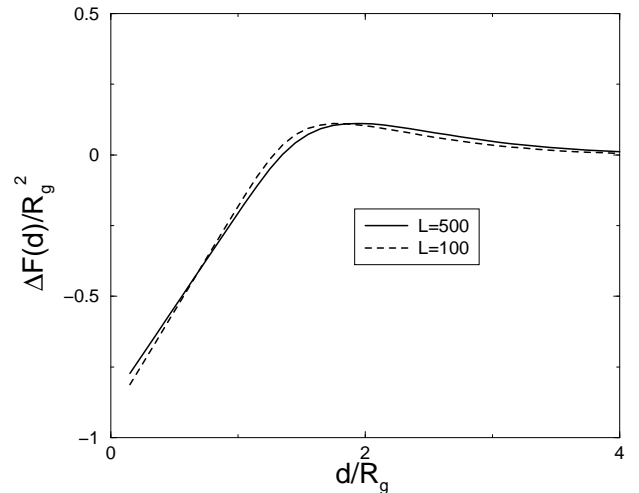


FIG. 20. Depletion free-energy $\Delta F(d)/R_g^2$ between two plates separated by d based on the soft particle representation for polymers of length $L = 100$ and $L = 500$. Here $\rho_b/\rho^* = 0.95$.

C. Comparison with the Asakura-Oosawa Approach

The first (and still most popular) approach to the depletion interaction in colloid-polymer mixtures was pioneered by Asakura and Oosawa in 1954 [25], when they approximated the polymers as ideal (Gaussian), and calculated the induced attraction between two walls. We shall refer to this neglect of polymer-polymer repulsion as the *AO approximation*, in contrast to the *AO model*, where a further step is taken and the polymers are approximated as inter-penetrating spheres of radius R_g [24].

The exact depletion potential induced by ideal polymers between two plates of area A a distance d apart is given by:

$$\Delta F(d)/A = \rho_b \Delta V_{id}(d), \quad (22)$$

where $\Delta V_{id}(d)$ is the gain in volume accessible to an ideal Gaussian polymer of size R_g , due to overlap of the exclusion volumes close to the plates. This can be exactly calculated as shown in the Appendix. To treat interacting polymers, a widely used phenomenological improvement (see for example ref. [10]) replaces the ideal polymer density by the bulk osmotic pressure Π_b of the interacting polymers in the left over free-volume:

$$\Delta F(d)/A = \Pi_b \Delta V_{id}(d). \quad (23)$$

In Fig. 21 we plot these two versions of the AO approximation for the largest density considered above, $\rho_b/\rho^* = 0.95$, and compare them to the effective potential and “exact” SAW simulation results. The two approaches result in rather poor representations of both the depth and the range of the true potential, even though we are technically not yet into the semi-dilute regime where one might expect them to break down (see also the inset of Fig. 18). For the lower densities the AO approximation works somewhat better, as expected.

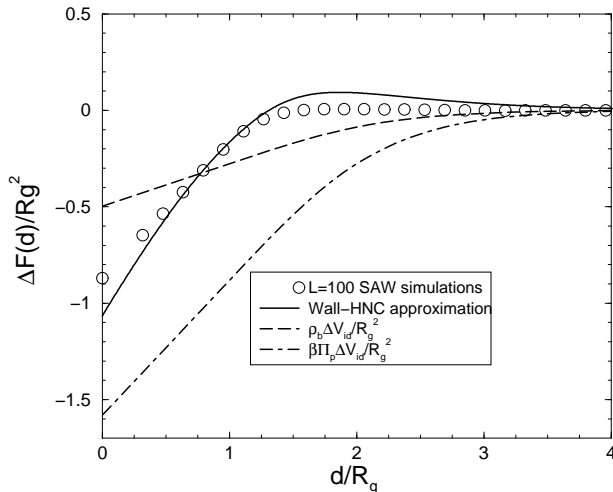


FIG. 21. Depletion free-energy $\Delta F(d)/R_g^2$ between two plates separated by d for $\rho_b/\rho^* = 0.95$. Circles are the “exact” MC simulations of SAW polymers. The long-dashed and dash-dotted lines denote the two AO approximations mentioned in the text. The short-dashed line denotes the more accurate wall-HNC approximation of Eq. (24), which is in fact very close to the the simulations in the soft particle picture shown in Fig. 18.

D. HNC Wall-Wall Approximation

Following arguments similar to those used to derive the wall-polymer HNC equations of section V B, one can also derive an HNC type equation for the depletion interaction free energy per unit area between two walls separated by a distance d [70]:

$$\frac{\Delta F(d)}{A} = -\rho_b \int_{-\infty}^{\infty} h(s)h(d-s)ds + \rho_b \int_{-\infty}^{\infty} h(d-s) [\phi(s; \rho_b) - \phi^{MF}(s; \rho_b)] ds. \quad (24)$$

Here $h(s) = \rho(s)/\rho_b - 1$ is the *single wall* density profile, $\phi(s; \rho_b)$ is the corresponding effective wall-polymer potential, and $\phi^{MF}(s; \rho_b)$ is the corresponding potential of mean force. The first term on the r.h.s. of Eq. (24) represents the density overlap approximation discussed in the Appendix, and is the only contribution in the case of ideal Gaussian polymer coils. The second term arises from correlations between the polymer coils, and dominates the first term for larger densities. Note that only information from one single wall enters into this HNC wall-wall approach. We use the effective wall-polymer potential $\phi(z; \rho_b)$ and the related density profile $h(z)$ from the soft-colloid picture together with Eq. (24) to derive the HNC wall-wall depletion free energy. As shown in Fig 21, this compares well with the MC simulations of the soft particles except at short distances where a small deviation develops that can be traced to the fact that only information from a single wall is used. A more promising approach, without this shortcoming, would be to directly use the MF or HNC DFT approaches applied in ref. [40] to Gaussian-core potentials.

VII. DISCUSSION AND CONCLUSION

The coarse-grained representation of polymer coils as soft colloids, put forward in this paper, has proved very reliable. The effective polymer-polymer and wall-polymer interactions obtained by a systematic inversion procedure based on fluid integral equations, yield pair distribution functions and concentration profiles which agree closely with the results from simulation of the full SAW segment model, while allowing a massive reduction in computer time compared to the lattice simulations.

Much of the success of the present coarse-graining procedure lies in our finding that the optimum effective pair potential between the CM's of neighboring coils does not depend strongly on polymer concentration, and is reasonably close to its infinite dilution limit. The effective polymer-polymer and wall-polymer interaction lead to a rather accurate description of the depletion interaction between two hard walls, despite the implicit potential superposition assumption and the fact that the coarse-graining procedure in its present form does not allow for the deformation of the polymer coils, away from the spherical shape, in the vicinity of an impenetrable surface. Such shape fluctuations are allowed in the alternative procedure by Murat and Kremer [28] but the remarkable agreement between the original full SAW model and the coarse-grained model illustrated in Fig. 18 seems to indicate that shape deformation of confined polymers may not be a crucial factor to reproduce concentration profiles.

The present inversion procedure yields concentration dependent effective pair potentials, but does not provide direct access to the internal free energy of polymer coils [28], which plays a role rather similar to that of the “self energy” or volume term of electric double-layers in charge-stabilized colloidal dispersions or solutions of star polymers [46]. This concentration-dependent term contributes to the osmotic equation of state, but the good agreement between full SAW model simulations and the results based on the effective pair interaction without the volume term would indicate that the concentration dependence of the latter is weak.

Finally, it must be stressed that the present inversion procedure is by no means restricted to the simple SAW model of non-intersecting polymers. We are in fact planning to extend the coarse-graining procedure to the case where the segment-segment coupling has an attractive component to describe the situation of polymer coils in poor solvent. The case of semi-dilute solutions of polymers of different lengths will also be considered within the same theoretical framework with the objective of studying possible demixing, as suggested by our recent investigation of binary Gaussian-core systems [40]. A final extension is to consider explicitly colloid-polymer mixtures, by determining the effective hard-sphere/polymer potential along the lines set out in this paper. The general methodology should, more generally, be applicable to dilute and semi-dilute solutions of linear, branched or star polymers in confined geometries.

ACKNOWLEDGEMENTS

AAL acknowledges support from the Isaac Newton Trust, Cambridge, PB acknowledges support from the EPSRC under grant number GR/M88839, EJM acknowledges support from the Royal Netherlands Academy of

Arts and Sciences. We thank David Chandler, Daan Frenkel, Ludger Harnau, Christos Likos, Hartmut Löwen, and Patrick Warren for helpful discussions.

APPENDIX A: DEPLETION POTENTIAL FOR IDEAL POLYMERS

In this Appendix we pursue a programme similar to that of the main text, but now for the simpler case of ideal Gaussian polymer coils of size R_g . Consider two parallel walls of area $A = L_x L_y$ a distance L_z apart. In the limit $L_x, L_y \gg R_g$, the full partition function for a single polymer is given by [25]:

$$Z_1 = L_x L_y L_z \frac{8}{\pi^2} \sum_{p=1,3,\dots}^{\infty} \frac{1}{p^2} \exp\left(-\frac{\pi^2 R_g^2 p^2}{L_z^2}\right). \quad (\text{A1})$$

From this, various properties, such as the depletion interaction between two walls, can be exactly calculated.

Similarly, from the underlying Green's function (see e.g. p. 19 of ref. [3]), the polymer end-point and mid-point density distributions near a single wall are found to be:

$$\frac{\rho_{\text{end}}^{(1)}(z)}{\rho_b} = \text{erf}\left(\frac{z}{2R_g}\right) \quad (\text{A2})$$

$$\frac{\rho_{\text{mid}}^{(1)}(z)}{\rho_b} = \left(\text{erf}\left(\frac{z}{\sqrt{2}R_g}\right)\right)^2. \quad (\text{A3})$$

As shown in Fig. 22, both show a clear depletion layer where polymer configurations are entropically excluded near the wall. In principle the CM distribution could also be calculated, but we have not yet succeeded in finding an analytic expression for it. Instead a polymer lattice model simulation with $L = 500$ was used to generate the $\rho_{\text{CM}}^{(1)}(z)$ depicted in Fig. 22.

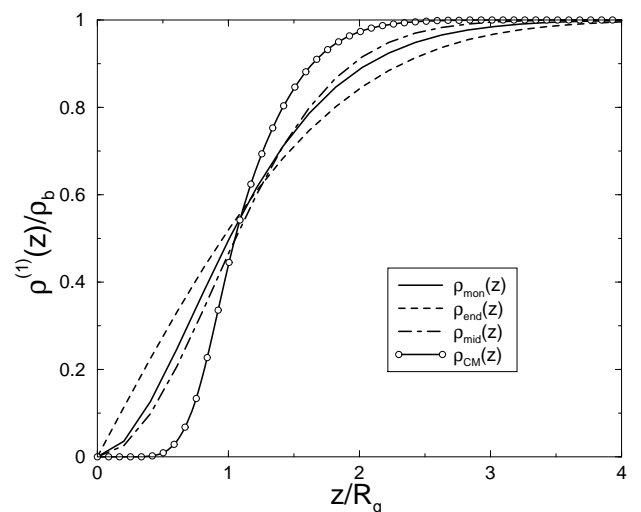


FIG. 22. Normalized densities $\rho^{(1)}(z)/\rho_b$ for ideal polymers near a wall. Also shown is the normalized monomer density [71] which falls, not unexpectedly, between the end and mid-point densities. The CM profile is the steepest since the CM cannot easily approach the wall as closely as the end or midpoints can.

Using either the end-points, mid-points or the CM as the centers of “effective particles”, an analogy with the full “soft particle” picture can be made. The particle-particle effective interaction is of course zero, while the effective particle-wall interaction can be inverted from the densities in Eqs. A2 and A3 with the result:

$$\phi_{end}^{(1)}(z) = -\ln \left[\text{erf} \left(\frac{z}{2R_g} \right) \right] \quad (\text{A4})$$

$$\phi_{mid}^{(1)}(z) = -2 \ln \left[\text{erf} \left(\frac{z}{\sqrt{2}R_g} \right) \right]. \quad (\text{A5})$$

The potential $\phi_{CM}^{(1)}(z)$ for the CM profile can be obtained numerically. In contrast to the soft-particle picture for interacting polymers, the inversion here is trivial, since for ideal particles the effective potential is simply the potential of mean force. The interaction $\phi_{CM}^{(1)}(z)$ for the Gaussian particles is in fact quite similar to the potential of mean force for SAW polymers at infinite dilution, shown in Fig. 16. But, whereas the wall-polymer interaction for interacting polymers changes with the bulk density, the $\phi^{(1)}(z)$ for Gaussian chains is independent of density.

Within the effective particle picture, two ways of calculating the interaction between two parallel walls are:
(1) the Potential Overlap Approximation (POA): Here the partition function of the effective particles confined between two walls, a distance L_z apart, is calculated for a total external potential given by:

$$\phi(z) = \phi^{(1)}(z) + \phi^{(1)}(L_z - z) \quad (\text{A6})$$

where z is the distance from one of the walls. For simple atomic or molecular fluids this superposition approximation would be exact and lead to the correct partition function and related equilibrium properties. However, for effective particles this is not necessarily the case as we shall see later on.

(2) the Density Overlap Approximation (DOA): Here the density between two parallel walls is approximated by the product of the densities near a single wall:

$$\rho_b \rho(z) = \rho^{(1)}(z) \rho^{(1)}(L_z - z) \quad (\text{A7})$$

In contrast to the POA, this approximation is incorrect even for simple atomic or molecular systems, although it is sometimes a useful first approximation. On the other hand, for ideal particles the POA and DOA approximations are equivalent.

The original Asakura Oosawa model [24] approximates the density profile $\rho^{(1)}(z)$ next to a single wall by a step function of range $R = R_g$. The depletion potential is then calculated within the DOA. This can be improved by adjusting the range of the step-function such that it excludes exactly the same amount of polymer as the true density profile. For flat walls this implies a step-function of range $R = 2R_g/\sqrt{\pi}$.

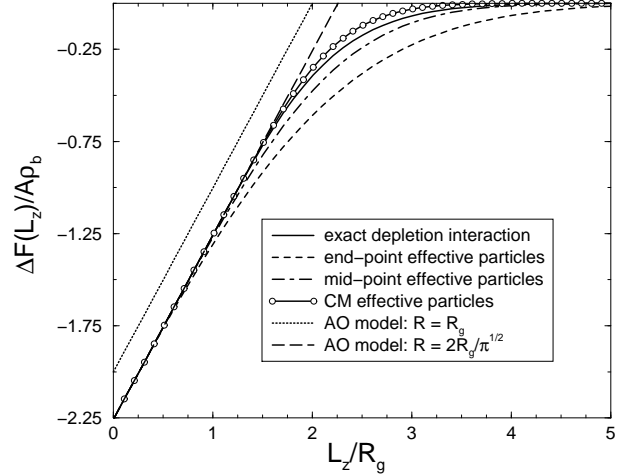


FIG. 23. A comparison of the normalized depletion interaction $\Delta F(L_z)/A\rho_b$ as a function of the wall-wall separation L_z/R_g for various approximations discussed in the text. The x-axis denotes.

In Fig. 23 we plot the depletion free-energy induced by non-interacting polymers between two walls a distance L_z apart. The exact expression was first calculated by Asakura and Oosawa [25]; here we approximate it by the following simple analytical expression:

$$\frac{\Delta F(L_z)}{A} = -\rho_b \left\{ \frac{4}{\sqrt{\pi}} - L_z \left(1 - \frac{8}{\pi^2} e^{-\frac{\pi^2 R_g^2}{L_z^2}} \right) \right\}; L_z < 4.332R_g$$

$$\frac{\Delta F(L_z)}{A} = 0; \quad L_z > 4.332R_g, \quad (\text{A8})$$

which arises from taking only the “ground state” of the partition function in Eq. (A1), and cutting the potential off where it crosses 0. This approximation is so accurate that the difference with the exact interaction cannot be resolved in Fig. 23. The effective particle representations, based on end-points, mid-points or the CM, provide a fairly good approximation to the full depletion interaction, while the two versions of the AO model do not perform as well.

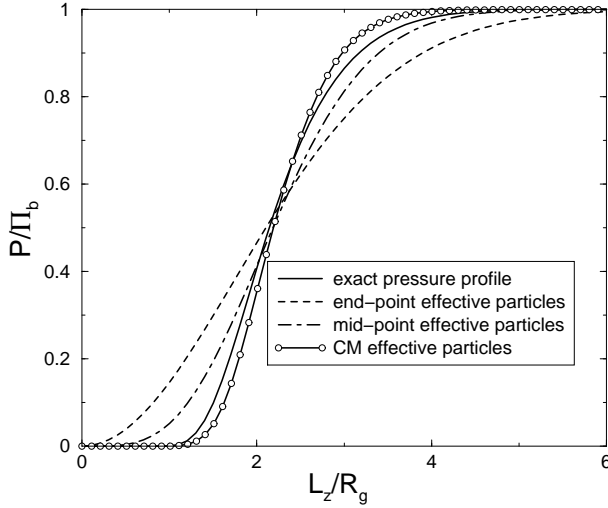


FIG. 24. Comparison of the reduced pressure $P(L_z; \mu)/\Pi_b$ between the walls as a function of wall-wall separation L_z/R_g . Π_b is the bulk pressure.

The pressure profiles shown in Fig. 24 demonstrate that the end and mid-point effective particle approaches underestimate the steepness of the pressure profile, while their CM counterpart overestimates the steepness. The differences between the effective particle representations and the exact results arise from our use of the POA. Because the underlying polymer configurations can easily extend to distances greater than $2R_g$, the POA, which implicitly assumes that the interaction of an effective particle with one wall is not directly affected by the presence of a second wall, begins to break down for strong confinement. Interestingly, the trend shown in Fig. 24 for the CM effective particle representation of the Gaussian coils mirrors the trend shown in Fig. 19 for interacting SAW polymers, suggesting that the differences for the latter also arise from the breakdown of the POA approximation.

We note that end-points or mid-points could also be used to construct an effective particle picture of interacting polymer solutions. For example, the mid-point representation would be very similar to the two-arm limit of a star-polymer, for which a number of results have been recently derived [57,59,63]. There are differences with the CM representation; for example, the mid-point equivalent of Eq. (4) would scale as [59,72]:

$$v_2(r) \sim -\frac{5\sqrt{2}}{9} \ln\left(\frac{r}{R}\right) \quad (\text{A9})$$

at short distances. Here R is a lengthscale proportional to the polymer size R_g . In contrast to the CM case, this interaction diverges at full overlap so that one would expect some qualitative differences in the behavior of the underlying soft particle fluids. However, the two approaches should, in principle, produce similar results for the thermodynamic properties of polymer solutions.

The relative merits of using mid-points v.s. the CM to describe polymer solutions are currently under investigation.

Finally we note that several results for ideal polymers, obtained here by using end-point or mid-point densities, can be also obtained by using the exact *monomer* density profiles near one wall [71] together with the DOA approximation [73].

-
- [1] P.J. Flory, *Principles of Polymer Chemistry* (Cornell University Press, Ithaca NY, 1953).
 - [2] P.G. de Gennes, *Scaling Concepts in Polymer Physics* (Cornell University Press, Ithaca NY, 1979).
 - [3] M. Doi and S.F. Edwards, *The Theory of Polymer Dynamics* (Oxford University Press, Oxford, 1986).
 - [4] J. des Cloizeaux and G. Jannink, *Polymers in Solution: Their Modelling and Structure* (Oxford University Press, Oxford, 1990).
 - [5] A.Y. Grosberg and A.R. Khokhlov, *Statistical Physics of Macromolecules* (AIP Press, New York, 1994).
 - [6] M. Doi, *Introduction to Polymer Physics* (Oxford University Press, Oxford, 1995).
 - [7] H.N.W. Lekkerkerker, W.C.K. Poon, P.N. Pusey, A. Stroobants and P.B. Warren, *Europhys. Lett.* **20**, 559 (1992).
 - [8] E.J. Meijer and D. Frenkel, *Phys. Rev. Lett.* **67**, 1110 (1991); *J. Chem. Phys.* **100**, 6873 (1994).
 - [9] R. Dickman and A. Yethiraj, *J. Chem. Phys.* **100**, 4683 (1994).
 - [10] S.M. Ilett, A. Orrock, W.C.K. Poon, and P.N. Pusey, *Phys. Rev. E*, **51**, 1344 (1995).
 - [11] Y.N. Ohshima *et al.* *Phys. Rev. Lett.* **78**, 3963 (1997).
 - [12] R. Verma, J.C. Crocker, T.C. Lubensky, and A.G. Yodh, *Phys. Rev. Lett.* **81**, 4004 (1998).
 - [13] A. Moussaid, W.C.K. Poon, P.N. Pusey, and M.F. Soliva, *Phys. Rev. Lett.* **82**, 225 (1999).
 - [14] W.C.K. Poon *et al.*, *Phys. Rev. Lett.* **83**, 1239 (1999).
 - [15] C. Bechinger, D. Rudhardt, P. Leiderer, R. Roth and S. Dietrich, *Phys. Rev. Lett.* **83**, 3960 (1999).
 - [16] A. Weiss, K. D. Hörner, and M. Ballauff, *J. Colloid Interface Sci.* **213**, 417 (1999).
 - [17] A. M. Kulkarni, A.P. Chatterjee, K.S. Schweizer, and C.F. Zukoski, *Phys. Rev. Lett.* **83**, 4554 (1999).
 - [18] A. Hanke, E. Eisenriegler and S. Dietrich, *Phys. Rev. E*, **59**, 6853 (1999).
 - [19] A. A. Louis, R. Finken, and J.P. Hansen, *Europhys. Lett.* **46**, 741 (1999); M. Dijkstra, J. Brader and R. Evans, *J. Phys.: Condens. Matter* **11**, 10079 (1999); M. Fuchs and K.S. Schweizer, preprint condmat/0007273.
 - [20] E.H.A. de Hoog, H.N.W. Lekkerkerker, J. Schulz, and G.H. Findenegg, *J. Phys. Chem. B* **103**, 10657 (1999).
 - [21] J. M. Brader and R. Evans, *Europhys. Lett.* **49**, 678 (2000).
 - [22] R. Tuinier, J.K.G. Dhont, and C.G. De Kruijf, *Langmuir* **16**, 1497 (2000).

- [23] P.J. Flory and W.R. Krigbaum, J. Chem. Phys. **18**, 1086 (1950).
- [24] S. Asakura and F. Oosawa, J. Polym. Sci., Polym. Symp. **33**, 183 (1958), A. Vrij, Pure Appl. Chem. **48**, 471 (1976).
- [25] S. Asakura and F. Oosawa, J. Chem. Phys. **22**, 1255 (1954).
- [26] F.K.R. Li-In-On, B. Vincent, and F. A. Waite, ACS Symp. Ser. **9**, 165 (1975).
- [27] A.A. Louis, P.G. Bolhuis, J.P. Hansen and E.J. Meijer, Phys. Rev. Lett. (2000), *in press*.
- [28] M. Murat and K. Kremer, J. Chem. Phys. **108**, 4340 (1998).
- [29] I. Carmesin and K. Kremer, Macromolecules **21**, 2819 (1988).
- [30] J. Dautenhahn and Carol K. Hall, Macromolecules **27**, 5399 (1994).
- [31] The crossover from dilute to semi-dilute solutions is not very sharply defined. We prefer to use $\rho^* = 3/(4\pi R_g^3)$. For a discussion favoring a slightly different definition see pp 593 of Ref. [4].
- [32] N. Madras and A.D. Sokal, J. Stat. Phys. **50** 109 (1988).
- [33] D. Frenkel and B. Smit, *Understanding molecular simulations* (Academic Press, 1995).
- [34] M. Dijkstra, D. Frenkel and J.P. Hansen, J. Chem. Phys. **101**, 3179 (1994).
- [35] S. Consta, T.J.H. Vlught, J.W. Hoeth, B. Smit, and D. Frenkel, Mol. Phys. **97**, 1243 (1999).
- [36] A.Y. Grosberg, P.G. Khalatur, and A.R. Khokhlov, Makromol. Chem., Rapid Commun. **3**, 709 (1982).
- [37] M. Daoud *et al.*, Macromolecules **8**, 804 (1975).
- [38] B. Krüger, L. Schäfer, and A. Baumgärtner, J. Phys. France **50**, 319 (1989).
- [39] O.F. Olaj, W. Lantschbauer, and K.H. Pelinka, Macromolecules **13** 299 (1980).
- [40] A.A. Louis, P. Bolhuis, and J.P. Hansen, preprint cond-mat/0007062.
- [41] B. Li, N. Madras, and A. Sokal, J. Stat. Phys. **80**, 661 (1995).
- [42] J. F. Douglas and K. F. Freed, Macromolecules **17**, 1854 (1984).
- [43] See for example pp. 77,78 of ref. [2], where the hard-sphere analogy is attributed to Flory (note, however, that this classic text was written before ref. [36]). In fact, B_2 scales with R_g^3 because that is the only lengthscale, not because the polymers exclude each other in a hard-sphere like fashion, a point which has also been emphasized by Schäfer [60,38].
- [44] R.L. Henderson, Phys. Lett. A. **49**, 197 (1974); J.T. Chayes and L. Chayes, J. Stat. Phys., **36**, 471 (1984).
- [45] L. Reatto, Phil. Mag. A **58**, 37 (1986); L. Reatto, D. Levesque, and J.J. Weis, Phys. Rev. A. **33**, 3451 (1986).
- [46] R. van Roij and J.P. Hansen, Phys. Rev. Lett. **79**, 3082 (1997); H. Graf and H. Löwen, Phys. Rev. E **57**, 5744 (1998); R. van Roij, M. Dijkstra and J.P. Hansen, Phys. Rev. E **59**, 2010 (1999); M. Dijkstra, R. van Roij and R. Evans, Phys. Rev. E. **59**, 5744 (1999).
- [47] G. Zerah, and J.P. Hansen, J. Chem. Phys. **84**, 2336 (1986)
- [48] J.P. Hansen and I.R. McDonald, *Theory of Simple Liquids*, 2nd Ed. (Academic Press, London, 1986).
- [49] Various techniques inspired by liquid state theory have been derived to treat polymers in the regime where monomer packing effects are important. See e.g. A. Yethiraj and C.E. Woodward, J. Chem. Phys. **102**, 5499 (1995), or K.S. Schweizer and J.G. Curro, Adv. Chem. Phys. **98**, 1 (1997) and references therein.
- [50] A. Hertanto and R. Dickman, J. Chem. Phys. **89**, 7577 (1988)
- [51] M.G. Bawendi and K.F. Freed, J. Chem. Phys. **88**, 2741 (1988)
- [52] R. J. Hanson, Sandia Labs. Tech. Rept. SAND-78-1291, December, (1978)
- [53] Parameters for the spline fits to the effective potentials are available from the authors.
- [54] W. Paul, K. Binder, D.W. Heermann, and K. Kremer, J. Phys. II **1**, 37 (1991).
- [55] F.H. Stillinger, J. Chem. Phys. **65**, 3968 (1976).
- [56] A. Lang, C.N. Likos, M. Watzlawek, and H. Löwen, J. Phys.: Condens. Matter **12**, 5087 (2000); C.N. Likos, A. Lang, M. Watzlawek, and H. Löwen, preprint cond-mat/0007089.
- [57] C. von Ferber *et al.*, Euro. Phys. J. E **2**, 311 (2000).
- [58] R. Dickman, J. Chem. Phys. **87**, 2246 (1987).
- [59] C.N. Likos, *Effective Interactions in Soft Condensed Matter Physics*, to appear in Physics Reports.
- [60] T. Ohta and Y. Oono, Phys. Lett. **89A**, 460 (1982), see also L. Schäfer, Macromolecules **15**, 652 (1982).
- [61] See Appendix A. of Y. Oono, Adv. Chem. Phys. **61**, 301 (1985).
- [62] P. Wiltzius, H.R. Haller, D. S. Cannell, and D.W. Schaefer, Phys. Rev. Lett. **51**, 1183 (1983).
- [63] C.N. Likos *et al.*, Phys. Rev. Lett. **89** 4450 (1998). M. Watzlawek, C.N. Likos, and H. Löwen, Phys. Rev. Lett. **82**, 5289 (1999).
- [64] J. van der Gucht, N. A. M. Besseling, J. van Male and M. A. Cohen Stuart, J. Chem. Phys. **113**, 2886 (2000).
- [65] R. Evans in D. Henderson ed., *Fundamentals of Inhomogeneous Fluids*, (Marcel Dekker, New York, 1992).
- [66] D.E. Sullivan and G. Stell, J. Chem. Phys. **69**, 5450 (1978).
- [67] E.J. Meijer *et al.*, *to be published*.
- [68] J. F. Joanny, L. Leibler, and P.G. de Gennes, J. Polym. Sci. Pol. Phys. **17**, 1073 (1979).
- [69] J.Y. Walz and A. Sharma, J. Colloid Interface Sci. **168**, 485 (1994); Y. Mao, M.E. Cates, and H.N.W. Lekkerkerker, Physica A, **222**, 10 (1995); B. Götzelmann, R. Roth, S. Dietrich, M. Dijkstra, and R. Evans, Europhys. Lett. **47**, 398 (1999); S. Melchionna and J.P. Hansen Phys. Chem. Chem. Phys. **2**, 3465 (2000).
- [70] P. Attard, D.R. Bérard, C.P. Ursenbach, and G.N. Patey, Phys. Rev. A **44**, 8224 (1991).
- [71] C.M. Marques and J.F. Joanny, Macromolecules **23**, 268 (1990).
- [72] T. Witten and P. A. Pincus, Macromolecules **19**, 2509 (1986).
- [73] R. Tuinier, G. A. Vliegthart, and H. N. W. Lekkerkerker, *preprint* (2000).